Insulin Resistance and Vulnerability to Cardiac Ischemia

Tomas Jelenik,[1,2] Ulrich Flögel,[3] Elisa Álvarez-Hernández,[1,2] Daniel Scheiber,[1,4] Elric Zweck,[1,4] Zhaoping Ding,[3] Maik Rothe,[1,2] Lucia Mastrototaro,[1,2] Vivien Kohlhaas,[1,2] Jörg Kotzka,[2,5] Birgit Knebel,[2,5] Dirk Müller-Wieland,[6] Sarah Moellendorf,[7] Axel Gödecke,[7] Malte Kelm,[4] Ralf Westenfeld,[4] Michael Roden,[1,2,8] and Julia Szendroedi[1,2,8]

Diabetes 2018;67:2695–2702 | https://doi.org/10.2337/db18-0449

Hepatic and myocardial ectopic lipid deposition has been associated with insulin resistance (IR) and cardiovascular risk. Lipid overload promotes increased hepatic oxidative capacity, oxidative stress, and impaired mitochondrial efficiency, driving the progression of nonalcoholic fatty liver disease (NAFLD). We hypothesized that higher lipid availability promotes ischemia-induced cardiac dysfunction and decreases myocardial mitochondrial efficiency. Mice with adipose tissue–specific overexpression of sterol element–binding protein 1c as model of lipid overload with combined NAFLD-IR and controls underwent reperfused acute myocardial infarcts (AMIs). Whereas indexes of left ventricle (LV) contraction were similar in both groups at baseline, NAFLD-IR showed severe myocardial dysfunction post-AMI, with prominent LV reshaping and increased end-diastolic and end-systolic volumes. Hearts of NAFLD-IR displayed hypertrophy, steatosis, and IR due to 18:1/18:1-diacylglycerol–mediated protein kinase Cε (PKCε) activation. Myocardial fatty acid–linked respiration and oxidative stress were increased, whereas mitochondrial efficiency was decreased. In humans, decreased myocardial mitochondrial efficiency of ventricle biopsies related to IR and troponin levels, a marker of impaired myocardial integrity. Taken together, increased lipid availability and IR favor susceptibility to ischemia-induced cardiac dysfunction. The diacylglycerol-PKCε pathway and reduced mitochondrial efficiency both caused by myocardial lipotoxicity may contribute to the impaired LV compensation of the noninfarcted region of the myocardium.

Insulin resistance (IR) and type 2 diabetes mellitus (T2DM) along with higher lipid availability associate with two- to fourfold greater cardiovascular mortality and myocardial vulnerability to ischemia-induced injury due to altered metabolism in noninfarcted regions (1).

Nonalcoholic fatty liver disease (NAFLD) independently relates to excessive cardiac mortality (2). Insulin-resistant humans feature hepatic mitochondrial adaptation with higher respiration but also reactive oxygen species (ROS) emission, which drives progression to nonalcoholic steatohepatitis (3,4). Whether such mechanisms are also operative within infarcted and/or remote myocardium after acute myocardial infarction (AMI), thereby contributing to higher heart vulnerability, is yet unclear. IR-related ischemic heart vulnerability may result from myocardial triglyceride and lipotoxin accumulation (5) or increased fatty acid utilization with impaired mitochondrial efficiency at the expense of higher oxygen demand (6,7).

We tested the hypotheses that NAFLD affects cardiac function post-AMI and induces lipid-associated myocardial IR with increased cardiac respiration and ROS emission but lower mitochondrial efficiency. We studied nonobese,

[1]Institute for Clinical Diabetology, German Diabetes Center, Düsseldorf, Germany
[2]German Center for Diabetes Research, München-Neuherberg, Germany
[3]Department of Molecular Cardiology, Medical Faculty, Heinrich-Heine University Düsseldorf, Düsseldorf, Germany
[4]Division of Cardiology, Pulmonology, and Vascular Medicine, Medical Faculty, Heinrich-Heine University Düsseldorf, Düsseldorf, Germany
[5]Institute for Biochemistry and Pathobiochemistry, German Diabetes Center, Düsseldorf, Germany
[6]Department of Medicine I, University Hospital Aachen, Aachen, Germany
[7]Department of Cardiovascular Physiology, Heinrich-Heine University Düsseldorf, Düsseldorf, Germany
[8]Division of Endocrinology and Diabetology, Medical Faculty, Heinrich-Heine University Düsseldorf, Düsseldorf, Germany

Corresponding author: Julia Szendroedi, julia.szendroedi@ddz.uni-duesseldorf.de.

Received 18 April 2018 and accepted 5 September 2018.

Clinical trial reg. no. NCT03386864, clinicaltrials.gov.

This article contains Supplementary Data online at http://diabetes.diabetesjournals.org/lookup/suppl/doi:10.2337/db18-0449/-/DC1.

nondiabetic mice with NAFLD and IR (8,9) and compared with age- and sex-matched controls. Second, we analyzed the mitochondrial function in the ventricular myocardium of humans with IR.

RESEARCH DESIGN AND METHODS

Animals

All studies were approved and performed according to guidelines in female 36-week-old mice with adipose tissue–specific overexpression of the SREBP-1c (NAFLD-IR) and C57Bl6 controls (CON). Mice had ad libitum access to standard diet and water.

AMI

Left anterior descending coronary artery was ligated and reperfused after 50 min of ischemia in anesthetized mice (10). Animals were analyzed before and 1, 2, 7, 14, 21, and 28 days post-AMI by cardiac MRI and spectroscopy (MRS).

Cardiac Magnetic Resonance Imaging and Spectroscopy

Data were recorded in a Bruker Avance III 9.4 Tesla Wide-Bore magnet (10). Respiration of anesthetized mice (1.5% isoflurane, 37°C) was monitored with a pneumatic pillow, and vital functions with the M1025 system (SA Instruments, Stony Brook, NY). Lipid content was quantified with a $1 \times 2 \times 3$ mm^3 voxel within the septum (Fig. 1*F*) and normalized to the water signal.

Hyperinsulinemic-Euglycemic Clamp

A silicon catheter was placed into the right-side jugular vein under anesthesia. Mice recovered for 4–5 days and were fasted for 6 h (3:00–9:00 A.M.). The clamp was performed with a primed (40 mU/kg) continuous infusion (4 mU/kg/min) (Huminsulin; Lilly, Giessen, Germany) for 180 min (8). Whole-body insulin sensitivity is expressed as glucose infusion rates (mg/kg/min).

High-Resolution Respirometry

O_2 fluxes were measured in isolated mitochondria and saponin-permeabilized left ventricle (LV) from mouse heart and permeabilized interventricular septum biopsies from human heart using Oxygraph-2k (Oroboros Instruments, Innsbruck, Austria) (11,12). H_2O_2 emission was monitored with the Amplex Red and Oxygraph-2k Fluorescence Module (8). Citrate synthase activity was

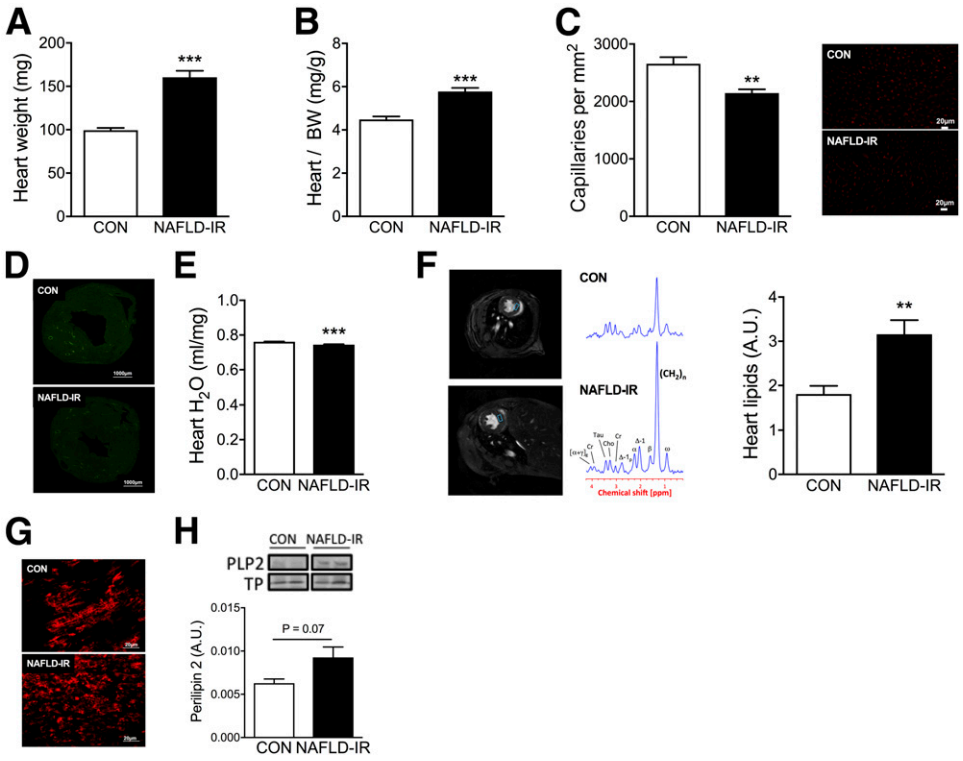

Figure 1—NAFLD associates with cardiac hypertrophy and increased lipid accumulation but no edema or fibrosis in the heart of NAFLD-IR mice. *A*: The heart weight (n = 7–9 per group). *B*: The ratio of the heart weight to body weight (BW) (n = 7–9 per group). *C*: Capillary density expressed as number of capillaries per square millimeter (left panel), as assessed from the immunohistochemical staining of the frozen myocardial tissue sections with anti-CD31 monoclonal antibodies (representative photographs shown in the right panel) (n = 10 per group). *D*: Representative photographs of the frozen myocardial tissue sections after immunohistochemical staining with anti–wheat germ agglutinin antibodies as a marker of fibrosis. *E*: Water content in the whole heart assessed with desiccation method (n = 5 per group). *F*: Cardiac lipids measured by ^{1}H-MRS in vivo (n = 8–10 per group). *G*: Representative photographs of the frozen myocardial tissue sections after immunohistochemical staining with anti–perilipin 2 antibodies as a marker of lipid droplets. *H*: Relative protein expression of perilipin 2 levels in the heart assessed with Western blots and normalized to total protein (TP) (n = 5 per group). All data are presented as mean ± SEM. $^{**}P < 0.01$ and $^{***}P < 0.001$, Student t test. A.U., arbitrary units.

assessed spectrophotometrically (Citrate Synthase Assay Kit; Sigma-Aldrich, St. Louis, MO) and proteins with fluorescamine.

Serum Oxidative Stress Markers

Serum thiobarbituric acid reactive substances (TBARS) were measured fluorometrically (BioTek, Bad Friedrichshall, Germany), catalase activity colorimetrically (Cayman Chemical Company), and static oxidation-reduction potential (sORP) and antioxidant capacity with RedoxSYS (Luoxis Diagnostics, Inc., Englewood, CO) (8).

Western Blots

Total protein was extracted from whole-heart homogenates. Differential centrifugation was used for membrane/cytosol separation (11). Specific antibodies were protein kinase Cε (PKCε), GLUT4, phospholamban (PLN), CHOP, and total protein kinase B (Akt) (Cell Signaling Technology, Danvers, MA).

Diacylglycerols

Cardiac diacylglycerol content and fatty acid composition were measured in the heart membrane/cytosol fractions with liquid chromatography—tandem mass spectrometry (13).

Histology

Hearts from anesthetized mice, washed in phosphate buffer and embedded in Tissue-Tek (O.C.T. Compound), were immediately frozen (−40°C) and stored (−80°C) until sectioning (14).

Capillary Density Calculation

Capillaries expressing CD31 were counted in two LV regions, measuring 250 × 400 μm and obtained at 20-fold magnification (http://imagej.nih.gov/ij; ImageJ software).

Laboratory Analyses

Tail blood glucose was measured with a glucometer (Precision Xtra Plus; Abbott, Wiesbaden, Germany), serum insulin with ELISA (Mercodia, Uppsala, Sweden), and serum triglyceride, cholesterol (Roche Diagnostics, Mannheim, Germany), and free fatty acid (Wako Chemicals, Neuss, Germany) photometrically.

Human Study

We enrolled 35 heart transplant recipients (Supplementary Table 2) with normal heart function, undergoing endomyocardial biopsy during posttransplantation allograft rejection monitoring. Intraventricular septum endomyocardial biopsies were taken catheter assisted (15). Exclusion criteria were allograft rejection, self-reported T2DM, diabetes-specific treatment, and/or fasting blood glucose >100 mg/dL and HbA_{1c} >6.5%. The HOMA-IR was calculated as previously described (16). The study was registered at clinicaltrials.gov (NCT03386864) and approved by the local ethics board.

Statistics

Data are presented as means ± SD in tables and text and as means ± SEM in figures. Groups were compared using unpaired two-tailed Student *t* test or two-way ANOVA with Holm-Sidak correction. The statistical significance threshold was $P < 0.05$.

RESULTS

Normotensive NAFLD-IR Mice Display Cardiac Hypertrophy and Steatosis

Metabolic characteristics of 6 h–fasted mice are shown in Supplementary Table 1. NAFLD-IR mice had 21% (Supplementary Table 1) and 61% higher body weight and heart weight (Fig. 1*A*) than CON. The heart-to-body weight ratio was higher (Fig. 1*B*) and heart capillary density was 19% lower (Fig. 1*C*), indicating cardiac hypertrophy. Arterial and LV blood pressure were comparable (Supplementary Fig. 1). Histology revealed intact cardiac tissue (Fig. 1*D*). Heart water content was 2% lower (Fig. 1*E*), whereas lipid content was 73% higher (Fig. 1*F*) in NAFLD-IR mice. Perilipin 2 staining showed irregularly distributed lipid droplets in NAFLD-IR hearts (Fig. 1*G*). Perilipin 2 protein content tended to be higher (Fig. 1*H*).

IR and Stimulation of the Diacylglycerol-PKCε Pathway in NAFLD-IR Heart

Whole-body insulin sensitivity was decreased in NAFLD-IR mice (Fig. 2*A*), due to reduced skeletal muscle and hepatic insulin sensitivity (8). Total cardiac AKT protein (Fig. 2*B*), membrane GLUT4 protein (Fig. 2*C*), and Pdk4 mRNA (Fig. 2*D*) were downregulated.

Total cardiac diacylglycerols were increased in membrane (Fig. 2*E*) and unchanged in cytosolic (Fig. 2*H*) fractions. Exclusively C18:1/C18:1-diacylglycerols increased in both fractions (Fig. 2*F* and *I*). PKCε increased in the membrane (Fig. 2*G*) and tended to decrease in the cytosol ($P = 0.063$) (Fig. 2*J*), yielding a doubled membrane-to-cytosolic PKCε ratio (0.52 ± 0.09 vs. CON 0.20 ± 0.01, $P < 0.0001$), indicating PKCε activation.

More Severe AMI-Induced LV Dysfunction in NAFLD-IR Mice

Infarct size was unchanged 1 day post-AMI (Fig. 3*A* and *B*), whereas cardiac function progressively declined in NAFLD-IR (Fig. 3*C*). LV mass was higher at baseline and remained higher post-AMI (Fig. 3*D*). Heart rate was comparable (Fig. 3*E*). LV end-diastolic and end-systolic volumes were comparable at baseline but increased more markedly in NAFLD-IR mice post-AMI (Fig. 3*F* and *G*). Systolic LV wall thickening was comparable at baseline but decreased more markedly in NAFLD-IR post-AMI (Fig. 3*H*). LV ejection fraction was comparable at baseline and impaired in both groups 2 days post-AMI (Fig. 3*I*). Impairment of ejection fraction was more severe in NAFLD-IR mice from day 7 on post-AMI.

Cardiac Mitochondrial Respiration and Oxidative Stress Are Increased in NAFLD-IR Mice at Baseline

At baseline, mitochondrial state 3 respiration was higher in NAFLD-IR with substrates providing electrons to complex I (pyruvate) and β-oxidation–linked electron-transferring flavoprotein complex (CETF; octanoyl-carnitine) (Fig. 4*A*).

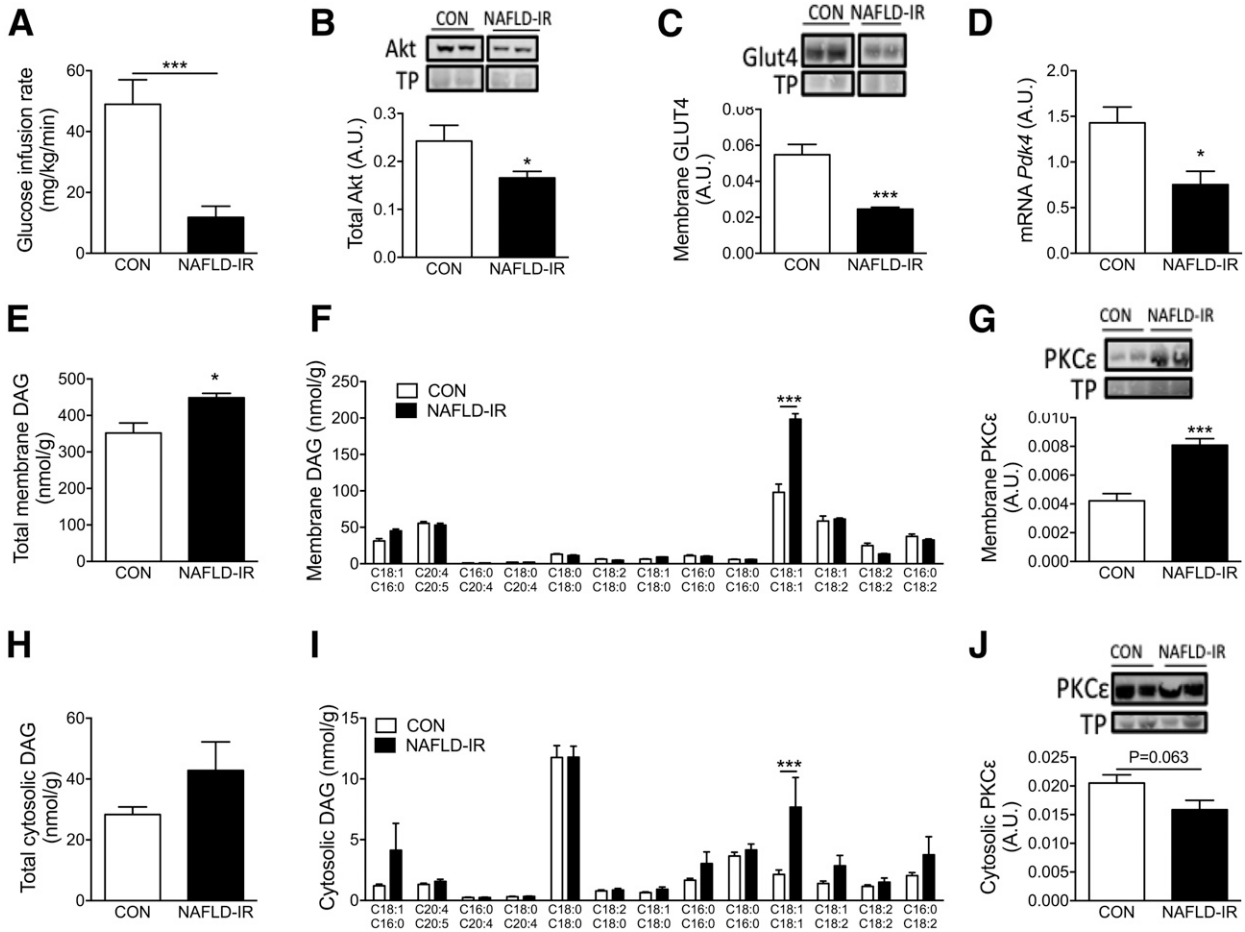

Figure 2— NAFLD-IR mice are characterized by decreased insulin sensitivity of the heart, paralleled by the induction of the diacylglycerol-PKCε pathway. *A*: Glucose infusion rate as an indicator of the whole-body insulin sensitivity was measured with hyperinsulinemic-euglycemic clamps (n = 5–7 per group). *B* and *C*: Relative protein expression of the Akt and membrane GLUT4 in the heart assessed with Western blots and normalized to total protein (TP) (n = 5 per group). *D*: Relative mRNA expression of *Pdk4* in the heart assessed with quantitative RT-PCR (n = 5 per group). *E* and *F*: Total diacylglycerol (DAG) levels in the membrane fraction of the heart and their fatty acid composition (n = 6–7 per group). *G*: Relative protein expression of the membrane PKCε in the heart assessed with Western blots and normalized to TP (n = 5 per group). *H* and *I*: Total DAG levels in the cytosolic fraction of the heart and their fatty acid composition (n = 6–7 per group). *J*: Relative protein expression of the cytosolic PKCε in the heart assessed with Western blots and normalized to TP (n = 5 per group). All data are presented as mean ± SEM. *$P < 0.05$ and ***$P < 0.001$, Student t test. A.U., arbitrary units.

H_2O_2 emission from complex III was 76% higher (Fig. 4*B*). Phosphate-to-oxygen ratios, indicating mitochondrial efficiency, decreased by 19% during β-oxidation–linked respiration (Fig. 4*C*).

On day 28 post-AMI, respiration decreased (Fig. 4*D*) and H_2O_2 emission increased (Fig. 4*E*) in the infarcted LV similarly in CON and NAFLD-IR. Serum sORP was elevated, whereas antioxidant capacity tended to be lower in NAFLD-IR post-AMI (Fig. 4*F*). Despite unchanged catalase activity (Fig. 4*G*), lipid peroxidation, assessed from TBARS, was increased in the serum of NAFLD-IR mice (Fig. 4*H*). Systemic inflammatory markers were comparable (8).

Decreased Markers of Contractility in the Heart of NAFLD-IR Mice at Baseline

The cardiac protein of sarco/endoplasmic reticulum Ca^{2+}-ATPase (SERCA2a) was comparable (Supplementary Fig. 2*A*), whereas its negative regulator PLN was higher (Supplementary Fig. 2*B*) in NAFLD-IR. Thus, the SERCA2a-to-PLN ratio, regulating calcium handling and fiber contractility, was decreased (Supplementary Fig. 2*C*). The CHOP protein, an indicator of endoplasmic reticulum stress and apoptosis, was comparable (Supplementary Fig. 2*D*).

IR Relates to Lower Myocardial Mitochondrial Efficiency in Human Myocardium

We tested the association between insulin sensitivity, myocardial integrity, and energy metabolism in 35 humans (Supplementary Table 2). LV ejection fraction by MRI or transthoracic echocardiography was 67.2 ± 1.5%. Whole-body IR (HOMA-IR) was 2.02 ± 0.20 and positively related to serum troponin T levels, a marker of reduced myocardial integrity (r = 0.40; P = 0.04; n = 26, Spearman test). HOMA-IR correlated negatively with respiratory control ratio linked to β-oxidation (CETF; octanoyl-carnitine) as well as to substrates of complex I and II and positively

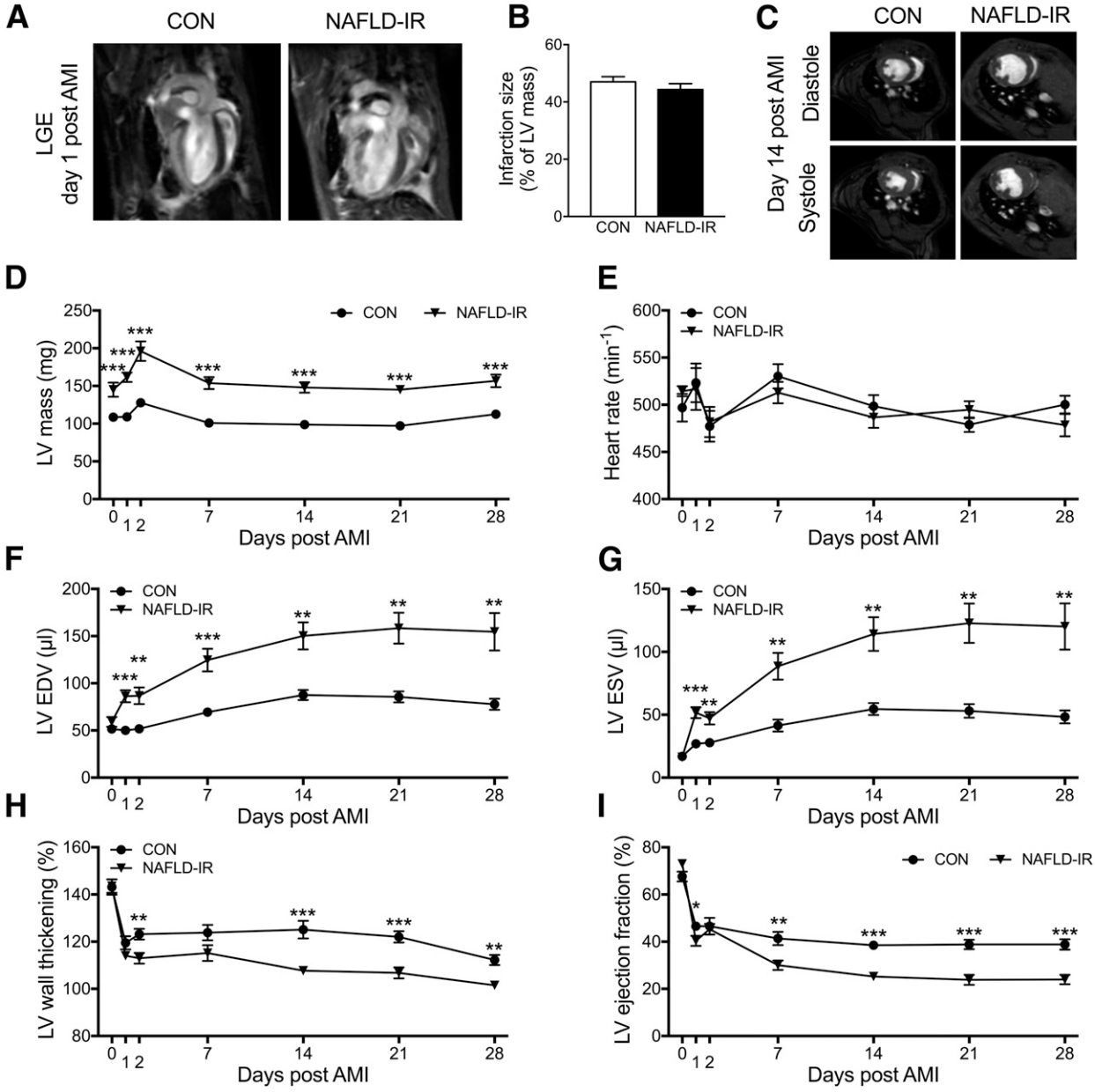

Figure 3—Cardiac morphology and function of NAFLD-IR mice at baseline and after AMI. *A*: Representative MRI with late gadolinium enhancement (LGE) showing the infarcted area (bright myocardium) on day 1 after AMI. *B*: Quantification of the infarction size on the day 1 post-AMI using LGE. *C*: Representative MRI of the end-diastole (upper panels) and end-systole (lower panels) hearts on day 14 post-AMI. *D*: LV mass. *E*: Heart rate. *F*: End-diastolic volume (EDV) of the LV. *G*: End-systolic volume (ESV) of the LV. *H*: The percent thickening of the LV wall with systole. *I*: Ejection fraction of the LV. All data are presented as mean ± SEM (n = 8–9 per group). *$P < 0.05$, **$P < 0.01$, and ***$P < 0.001$ between genotypes matched for time (multiple Student t test).

with the leak control ratio (Supplementary Fig. 3). Thus, lower insulin sensitivity associates with lower ventricular mitochondrial coupling and efficiency. Also serum troponin T correlated with respiratory control ratio and leak control ratio (Supplementary Fig. 3), suggesting that impaired myocardial integrity relates to lower mitochondrial efficiency.

DISCUSSION

This study shows that IR, NAFLD, and cardiac steatosis, even in the absence of overt T2DM, associate with greater impairment of cardiac function post-AMI. The underlying mechanisms comprised the accumulation of 18:1 fatty acid–containing diacylglycerols, PKCε-mediated IR, and lipid-induced upregulation of mitochondrial respiration and ROS emission, but lower mitochondrial coupling and efficiency. In humans, coupling and efficiency of the mitochondria from the ventricular myocardium also declined with IR and associated with impaired myocardial integrity.

NAFLD-IR mice featured severe AMI-induced myocardial dysfunction with LV reshaping and higher end-diastolic

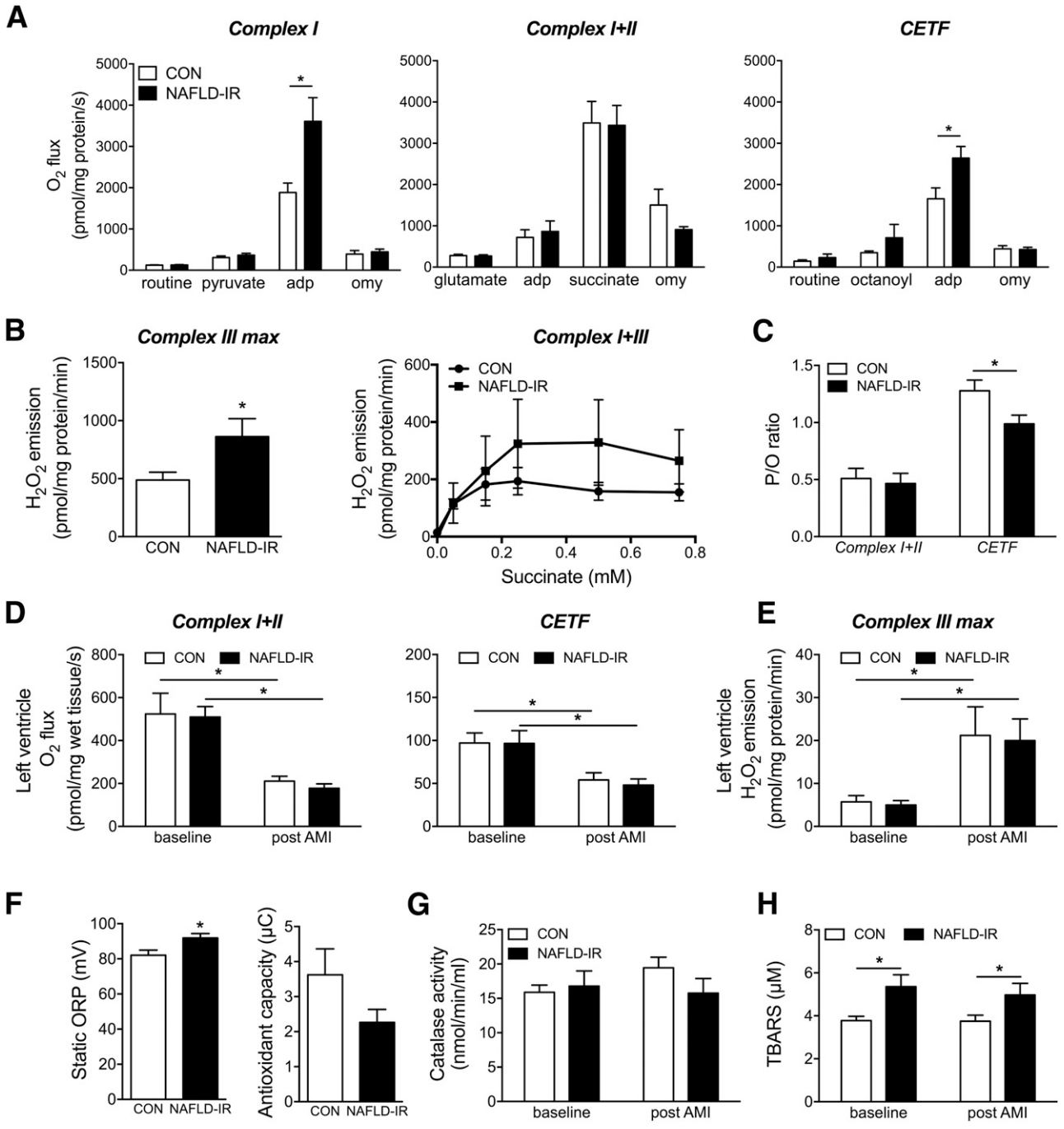

Figure 4—Mitochondrial respiration and oxidative stress in the heart of NAFLD-IR mice at baseline conditions and after AMI. *A*: Oxygen consumption linked to complex I (pyruvate and glutamate), complex II (succinate), and electron transfer flavoprotein complex (CETF; octanoyl-carnitine) at state 3 (adp) and state 4o (oligomycin [omy]) respiration in isolated heart mitochondria (n = 7–8 per group). *B*: H_2O_2 emission from complex III (antimycin) and dose-response curves of succinate-stimulated H_2O_2 emission in isolated heart mitochondria (n = 8 per group). *C*: Phosphate-to-oxygen (P/O) ratio, an indicator of the mitochondrial efficiency, assessed by dividing the moles of ADP phosphorylated to ATP by the moles of atomic oxygen consumed by isolated heart mitochondria (n = 5 per group). *D*: Oxygen consumption linked to complex I + II (pyruvate, glutamate, and succinate) and CETF (octanoyl-carnitine) at state 3 (adp) respiration was assessed in permeabilized left heart ventricles at baseline and 28 days after AMI (n = 5–10 per group). *E*: H_2O_2 emission from complex III (antimycin) was assessed in permeabilized LV at baseline and 28 days post-AMI (n = 5–10 per group). *F*: sORP and antioxidant capacity assessed in serum from mice 28 days post-AMI (n = 7–8 per group). *G*: Catalase activity in the serum of mice at baseline and 28 days post-AMI (n = 5–10). *H*: Concentrations of TBARS in the serum of mice at baseline and 28 days post-AMI (n = 5–10 per group). All data are presented as mean ± SEM. *$P < 0.05$, Student t test or two-way ANOVA.

and end-systolic volumes. Capillary density was lower, probably reflecting cardiomyocyte hypertrophy and/or failure of compensatory angiogenesis (17). Arterial pressure and heart rate were unaffected. Cardiac hypertrophy was not accompanied by fibrosis or edema. Cardiac lipids increased probably due to similar mechanisms as in the liver and muscle (8), i.e., by unsuppressed fat lipolysis and increased lipid uptake. These findings are in line with observations in patients with T2DM (18–20) and patients without diabetes with NAFLD (21).

Cardiac steatosis in NAFLD-IR was paralleled by higher diacylglycerol and membrane PKCε concentrations. Diacylglycerols activate novel PKCs, PKCε and θ, which impair hepatic and muscle insulin signaling and may also affect cardiac remodeling and a variety of cardiac diseases (22). The current study identified accumulation of oleic acid (C18:1/C18:1)–containing diacylglycerols, being in line with the concept that unsaturated diacylglycerols are more potent activators of novel PKCs (23). Mice with cardiac-specific PKCε overexpression develop impaired cardiac function (24). Thus, the diacylglycerol/PKCε pathway could contribute to LV dysfunction of NAFLD-IR mice post-AMI.

In IR and NAFLD, mitochondrial respiration increases in the livers of humans (3) and mice (8) as an adaptation to higher substrate availability, leading to lower mitochondrial ATP production (3,4,25). We found higher mitochondrial respiration and ROS emission in the hearts of NAFLD-IR. Increased ROS can alter calcium handling in heart failure via SERCA2a inhibition (26). Indeed, the cardiac SERCA2a-to-PLN ratio decreased in NAFLD-IR. Furthermore, oxidative damage can induce intracellular damage, leading to apoptosis. Accordingly, mitochondrial efficiency was lower in the heart of NAFLD-IR mice. This could contribute to the effects of IR, i.e., preferential fatty acid oxidation, which is energetically less efficient (27), in turn leading to impaired cardiac function during higher energy demands and lower oxygen supply, such as after AMI.

In humans, myocardial ventricular mitochondrial efficiency negatively associated with IR. Previously, controversial results have been obtained in the atrial myocardium of obese humans and patients with T2DM (28). In this study, human ventricular myocardium featured a similar mitochondrial phenotype as myocardium of NAFLD-IR mice. In particular, decreased coupling and efficiency of the mitochondria from the human ventricular myocardium paralleled decreasing insulin sensitivity. Moreover, serum troponin T levels associated negatively with myocardial mitochondrial efficiency. Circulating troponin is not only a common marker of myocardial ischemia but also a prognostic factor of myocardial damage even in the absence of myocardial infarction (29). Similar to the lower AMI tolerance in NAFLD-IR mice, the lower mitochondrial efficiency could contribute to higher myocardial damage in insulin-resistant humans.

In conclusion, mice with IR and NAFLD due to ectopic lipid accumulation show myocardial steatosis, lipid-induced changes of cardiac metabolism, and induction of the C18:1/C18:1-diacylglycerol-PKCε pathway, leading to severe myocardial dysfunction post-AMI and impaired insulin signaling. Cardiac mitochondria adapt to lipid accumulation by increased respiration, which associates with increased ROS emission and less efficient energy production, as supported by the human data. Collectively, these mechanisms operative in lipid-induced IR contribute to the impaired LV compensation post-AMI.

Acknowledgments. The authors thank Gerald I. Shulman and Mario Kahn (Yale University School of Medicine, New Haven, CT), Katharina Bottermann (Department of Cardiovascular Physiology, Heinrich-Heine University Düsseldorf), and Ilka Rokitta and Olesja Ritter (Institute for Clinical Diabetology, German Diabetes Center) for their excellent help and support.

Funding. This study was supported by the German Research Foundation (DFG, SFB 1116), the Ministry of Science and Research of the State of North Rhine-Westphalia (MIWF NRW), the German Federal Ministry of Health (BMG), the Federal Ministry for Research (BMBF) to the German Center for Diabetes Research (DZD e.V.), the German Diabetes Association (DDG), the Schmutzler-Stiftung, and the National Institutes of Health/National Institute of Diabetes and Digestive and Kidney Diseases (R01-DK-40936, U24-DK-059635, and P30-DK-45735).

Duality of Interest. No potential conflicts of interest relevant to this article were reported.

Author Contributions. T.J. conceived of the experiments, researched data, contributed to the discussion, and wrote the manuscript. U.F., E.Á.-H., D.S., E.Z., and L.M. researched data and contributed to the discussion. Z.D., M.Rot., V.K., J.K., and S.M. researched data. B.K., D.M.-W., A.G., M.K., and R.W. contributed to the discussion. M.Rod. and J.S. conceived of the experiments, contributed to the discussion, and wrote the manuscript. J.S. is the guarantor of this work and, as such, had full access to all the data in the study and takes responsibility for the integrity of the data and the accuracy of the data analysis.

Prior Presentation. This study was presented at the 72nd Scientific Sessions of the American Diabetes Association, Philadelphia, PA, 8–12 June 2012, and the 78th Scientific Sessions of the American Diabetes Association, Orlando, FL, 22–26 June 2018.

References

1. Rubler S, Dlugash J, Yuceoglu YZ, Kumral T, Branwood AW, Grishman A. New type of cardiomyopathy associated with diabetic glomerulosclerosis. Am J Cardiol 1972;30:595–602

2. Byrne CD, Targher G. NAFLD: a multisystem disease. J Hepatol 2015;62 (Suppl.):S47–S64

3. Koliaki C, Szendroedi J, Kaul K, et al. Adaptation of hepatic mitochondrial function in humans with non-alcoholic fatty liver is lost in steatohepatitis. Cell Metab 2015;21:739–746

4. Tilg H, Moschen AR, Roden M. NAFLD and diabetes mellitus. Nat Rev Gastroenterol Hepatol 2017;14:32–42

5. Goldberg IJ, Trent CM, Schulze PC. Lipid metabolism and toxicity in the heart. Cell Metab 2012;15:805–812

6. Buchanan J, Mazumder PK, Hu P, et al. Reduced cardiac efficiency and altered substrate metabolism precedes the onset of hyperglycemia and contractile dysfunction in two mouse models of insulin resistance and obesity. Endocrinology 2005;146:5341–5349

7. Mazumder PK, O'Neill BT, Roberts MW, et al. Impaired cardiac efficiency and increased fatty acid oxidation in insulin-resistant ob/ob mouse hearts. Diabetes 2004;53:2366–2374

8. Jelenik T, Kaul K, Séquaris G, et al. Mechanisms of insulin resistance in primary and secondary nonalcoholic fatty liver. Diabetes 2017;66:2241–2253

9. Shimomura I, Hammer RE, Richardson JA, et al. Insulin resistance and diabetes mellitus in transgenic mice expressing nuclear SREBP-1c in adipose

tissue: model for congenital generalized lipodystrophy. Genes Dev 1998;12:3182–3194
10. Flögel U, Ding Z, Hardung H, et al. In vivo monitoring of inflammation after cardiac and cerebral ischemia by fluorine magnetic resonance imaging. Circulation 2008;118:140–148
11. Jelenik T, Séquaris G, Kaul K, et al. Tissue-specific differences in the development of insulin resistance in a mouse model for type 1 diabetes. Diabetes 2014;63:3856–3867
12. Phielix E, Jelenik T, Nowotny P, Szendroedi J, Roden M. Reduction of non-esterified fatty acids improves insulin sensitivity and lowers oxidative stress, but fails to restore oxidative capacity in type 2 diabetes: a randomised clinical trial. Diabetologia 2014;57:572–581
13. Neschen S, Morino K, Hammond LE, et al. Prevention of hepatic steatosis and hepatic insulin resistance in mitochondrial acyl-CoA:glycerol-sn-3-phosphate acyltransferase 1 knockout mice. Cell Metab 2005;2:55–65
14. Emde B, Heinen A, Gödecke A, Bottermann K. Wheat germ agglutinin staining as a suitable method for detection and quantification of fibrosis in cardiac tissue after myocardial infarction. Eur J Histochem 2014;58:2448
15. Anderson JL, Marshall HW. The femoral venous approach to endomyocardial biopsy: comparison with internal jugular and transarterial approaches. Am J Cardiol 1984;53:833–837
16. Wallace TM, Levy JC, Matthews DR. Use and abuse of HOMA modeling. Diabetes Care 2004;27:1487–1495
17. Rakusan K, Flanagan MF, Geva T, Southern J, Van Praagh R. Morphometry of human coronary capillaries during normal growth and the effect of age in left ventricular pressure-overload hypertrophy. Circulation 1992;86:38–46
18. Goland S, Shimoni S, Zornitzki T, et al. Cardiac abnormalities as a new manifestation of nonalcoholic fatty liver disease: echocardiographic and tissue Doppler imaging assessment. J Clin Gastroenterol 2006;40:949–955
19. Fotbolcu H, Yakar T, Duman D, et al. Impairment of the left ventricular systolic and diastolic function in patients with non-alcoholic fatty liver disease. Cardiol J 2010;17:457–463
20. Mantovani A, Zoppini G, Targher G, Golia G, Bonora E. Non-alcoholic fatty liver disease is independently associated with left ventricular hypertrophy in hypertensive type 2 diabetic individuals. J Endocrinol Invest 2012;35:215–218
21. Cassidy S, Hallsworth K, Thoma C, et al. Cardiac structure and function are altered in type 2 diabetes and non-alcoholic fatty liver disease and associate with glycemic control. Cardiovasc Diabetol 2015;14:23
22. Palaniyandi SS, Sun L, Ferreira JC, Mochly-Rosen D. Protein kinase C in heart failure: a therapeutic target? Cardiovasc Res 2009;82:229–239
23. Madani S, Hichami A, Legrand A, Belleville J, Khan NA. Implication of acyl chain of diacylglycerols in activation of different isoforms of protein kinase C. FASEB J 2001;15:2595–2601
24. Takeishi Y, Ping P, Bolli R, Kirkpatrick DL, Hoit BD, Walsh RA. Transgenic overexpression of constitutively active protein kinase C epsilon causes concentric cardiac hypertrophy. Circ Res 2000;86:1218–1223
25. Szendroedi J, Chmelik M, Schmid AI, et al. Abnormal hepatic energy homeostasis in type 2 diabetes. Hepatology 2009;50:1079–1086
26. Kubin AM, Skoumal R, Tavi P, et al. Role of reactive oxygen species in the regulation of cardiac contractility. J Mol Cell Cardiol 2011;50:884–893
27. Lopaschuk GD, Ussher JR, Folmes CD, Jaswal JS, Stanley WC. Myocardial fatty acid metabolism in health and disease. Physiol Rev 2010;90:207–258
28. Montaigne D, Marechal X, Coisne A, et al. Myocardial contractile dysfunction is associated with impaired mitochondrial function and dynamics in type 2 diabetic but not in obese patients. Circulation 2014;130:554–564
29. Zethelius B, Johnston N, Venge P. Troponin I as a predictor of coronary heart disease and mortality in 70-year-old men: a community-based cohort study. Circulation 2006;113:1071–1078